DETERMINATION OF THE GOLD ALLOYS COMPOSITION BY LASER-INDUCED PLASMA SPECTROSCOPY USING AN ALGORITHM FOR MATCHING EXPERIMENTAL AND CALCULATED VALUES OF ELECTRON NUMBER DENSITY**

Zahid Farooq [1*], Raheel Ali [2*], Nasar Ahmed [3], Muhammad Fahad [4], Aqrab ul Ahmad [5], Muhammad Yaseen [6], Mian H. R. Mahmood [6], Sajjad Hussain [1], I. Rehan [7], M. Zubair Khan [7], Tariq Jan [8], Muhammad Abdul Qayyum [6], Muhammad Afzal [9], Muhammad Shabir Mahr [10], Muhammad Shafique [10]

[1] Department of Physics, Division of Science & Technology, University of Education, Lahore, Pakistan; e-mail: zahidv13@hotmail.com
[2] Department of Physics, Quaid-e-Azam University, Islamabad, Pakistan
[3] Department of Physics, University of Azad Jammu and Kashmir, Muzaffarabad, Pakistan
[4] Department of Electrical and Computer Engineering, COMSATS University, Islamabad, Abbottabad Campus, Abbottabad, Pakistan
[5] Department of Physics, Riphah International University, Faisalabad Campus, Faisalabad, Pakistan
[6] Department of Chemistry, Division of Science & Technology, University of Education, Lahore, Pakistan
[7] Department of Physics, Islamia College University, Peshawar, Pakistan
[8] Department of Physics, Allama Iqbal Open University, Islamabad, Pakistan,
[9] Department of Mathematics, Division of Science & Technology, University of Education, Lahore, Pakistan
[10] Department of Physics, University of Agriculture, Faisalabad, Pakistan

Laser-induced breakdown spectroscopy (LIBS) was applied for qualitative and quantitative analysis of gold alloys. A frequency double-pulsed Nd:YAG laser was used to generate plasma on the surface of gold alloys. The plasma temperatures of gold and copper were calculated using Boltzmann plots whereas electron number densities were determined via Saha–Boltzmann equations. The effect of self-absorption in the laser-induced emission spectra was evaluated for correction in the intensity of spectral lines. By combining electron number density conservation approach (ENDC) with LIBS, an algorithm for gold alloys composition determination was derived by matching the theoretically derived ratios of the number densities and the experimentally obtained ratios of the number densities extracted from LIBS spectra. The results of ENDC-LIBS approach were compared with those estimated by a conventional calibration-free LIBS approach and other established analytical technique energy dispersive X-ray. The results clearly demonstrated that ENDC-LIBS methodology appeared to be very promising for analysis of LIBS spectra of gold alloys.

Keywords: *laser-induced breakdown spectroscopy, gold alloys, laser-induced plasma, self-absorption, electron number density conservation approach.*

**Full text is published in JAS V. 90, No. 1 (http://springer.com/journal/10812) and in electronic version of ZhPS V. 90, No. 1 (http://www.elibrary.ru/title_about.asp?id=7318; sales@elibrary.ru).

ОПРЕДЕЛЕНИЕ СОСТАВА СПЛАВОВ ЗОЛОТА МЕТОДОМ СПЕКТРОСКОПИИ ЛАЗЕРНО-ИНДУЦИРОВАННОЙ ПЛАЗМЫ С ИСПОЛЬЗОВАНИЕМ АЛГОРИТМА СОГЛАСОВАНИЯ ЭКСПЕРИМЕНТАЛЬНЫХ И РАССЧИТАННЫХ ЗНАЧЕНИЙ ЭЛЕКТРОННОЙ ПЛОТНОСТИ

Z. Farooq [1*], R. Ali [2*], N. Ahmed [3], M. Fahad [4], A. ul Ahmad [5], M. Yaseen [6], M. H. R. Mahmood [6], S. Hussain [1], I. Rehan [7], M. Z. Khan [7], T. Jan [8], M. A. Qayyum [6], M. Afzal [9], M. S. Mahr [10], M. Shafique [10]

УДК 543.423:546.59

[1] Отделение физики Образовательного университета, Лахор, Пакистан; e-mail: zahidv13@hotmail.com
[2] Университет Куэйд-и-Азам, Исламабад, Пакистан
[3] Университет Азад Джамму и Кашмира, Музаффарабад, Пакистан
[4] Университет COMSATS, Исламабад, Абботтабад, Пакистан
[5] Международный университет Рифа, Фейсалабад, Пакистан
[6] Образовательный университет, Лахор, Пакистан
[7] Отделение физики Исламского колледжа, Пешавар, Пакистан
[8] Университет имени Алламы Икбала, Исламабад, Пакистан
[9] Отдел науки и технологий Образовательного университета, Лахор, Пакистан
[10] Сельскохозяйственный университет, Фейсалабад, Пакистан

(Поступила 29 марта 2022)

Лазерно-искровая эмиссионная спектроскопия (LIBS) применена для качественного и количественного анализа сплавов золота. Для генерации плазмы на поверхности сплавов золота использован импульсный Nd:YAG-лазер с удвоенной частотой излучения. Температуры плазмы золота и меди рассчитаны с помощью графиков Больцмана, электронная плотность — с помощью уравнений Саха–Больцмана. Эффект самопоглощения в спектрах лазерно-индуцированного излучения оценен для коррекции интенсивности спектральных линий. Комбинированием подхода сохранения электронной плотности (ENDC) с LIBS разработан алгоритм определения состава сплавов золота путем сопоставления теоретических рассчитанных и полученных из LIBS-спектров значений электронной плотности. Сравнение результатов, полученных методом ENDC-LIBS и с помощью обычного подхода LIBS без калибровки и другого общепринятого аналитического подхода энергодисперсионного рентгеновского анализа, показало перспективность подхода ENDC-LIBS для анализа LIBS-спектров сплавов золота.

Ключевые слова: *лазерно-искровая эмиссионная спектроскопия, сплавы золота, лазерно-индуцированная плазма, самопоглощение, подход сохранения электронной плотности.*

Introduction. Laser-induced breakdown spectroscopy (LIBS) is a recognized analytical tool suitable for a rapid and online multi-elemental analysis of any type of material [1, 2]. Its potential applications have been established in the investigation of contaminants, toxic elements and pollutants in diverse types of matrices, even those present under tough environmental conditions. In this technique, a powerful laser pulse with sufficient energy is focused on any material (i.e., solid, liquid, and gas), resulting in the vaporization and ionization of material in hot plasma, which is later analyzed by the LIBS spectrometer.

Various theoretical approaches to LIBS emission spectra have been used to raise the sensitivity of the LIBS technology. This includes calibration-based [3, 4] and calibration-free LIBS approaches [5, 6]. The first, the calibration-based approach, demands the drawing of calibration curves and requires a set of standards for quantitative analysis. The calibration-based approach was replaced by a self-calibration or calibration-free approach. The self-calibration method was initially originated by Ciucci et al. [7] in which concentration is estimated with the help of the Boltzmann plot, where a slope estimates the plasma temperature whereas the intercept guides us to estimate the concentration of species. Later, Yang et al. [8] proposed a method based on the auto selection of an internal reference line. A lot of quantitative work has already been done using this calibration-free (CF) approach [9, 10]. The major disadvantage of these methods is that it is hard to produce the Boltzmann plot for all the species owing to the unavailability of a sufficient number

of spectral lines. To overcome these problems, a new approach to the electron number density (END) conservation was introduced by Gomba et al. [11]. They estimated the contents of material by using the relative number densities of the neutral and singly ionized ionic species. In the current study, an END conservation LIBS approach based on an algorithm was applied to LIBS spectra of gold alloys without any external calibrations.

Gold is a precious metal and its purity is typically marked by the gold alloys, which are called carat gold (from 8 to 24 carat). Carat gold is mostly alloy consisting of gold with copper compositions. High grade of precision for composition of gold alloys is required for diverse tasks coupled with process control in the gold industry. The composition analysis of different grades of gold is a labor-intensive process because it is treated in traditional ways that are very complex [12–14]. These conventional methods have a lot of faults, including the destruction of material, the limitation of adequate reference materials, and low accuracy. To overcome these issues, several other techniques have been introduced that are nondestructive in nature but require working standards and possession of adequate reference materials; therefore, there is a dire need to establish a nondestructive analytical technique. X-ray fluorescence (XRF) has appeared to be a good alternative but it has some constraints such as surface smoothness and depth profiling (~1–2 μm) [15]. In recent decades, LIBS has proved to be a better alternative to the above-mentioned techniques. It is useful for the elemental analysis of composition of various grades of gold (from 8 to 24 carat) and gold alloys (jewelry, coinage, etc.). Over the last few decades, there have been significant contributions reported regarding LIBS of carat gold. However, there are a number of uncertainties reported in the results of LIBS methodologies due to matrix effect, self-absorption, and other experimental constraints. The main two aims of the current study were, first, a to apply self-absorption correction to LIBS spectra of gold alloys in order to utilize the real value of intensity of LIBS spectra for estimation [16, 17]. Later, an END conservation approach was applied to LIBS spectra of proposed samples of gold to improve the analytical performance of LIBS for gold alloys. The results of the END conservation LIBS approach have been compared with those obtained from conventional CF-LIBS approach and other established analytical techniques exhibiting good agreement. Two samples of gold alloys (i.e., 22 and 18 carat gold samples) were investigated for their content of gold and copper.

Experimental set-up and data acquisition. The experimental set-up and apparatus in the present study is almost the same as that described in our earlier studies [18]. A conventional LIBS experimental set-up consists of Nd:YAG laser (Quantel Brilliant, France), delay generator, focusing optics, rotated stand for sample target, spectrometer, and signal detection system. In brief, a Nd:YAG laser (Quantel, Brilliant B) having 300 mJ laser energy at 532 nm was operated at a 10-Hz repetition rate and 5-ns pulse duration. The laser pulse energy was varied by the *Q*-switch delay, and its energy was measured by an energy meter. The laser beam with 100-mJ pulse energy was focused on the surface of the sample using a 20-cm focusing lens placed perpendicular to the target sample. The power density was adjusted about 10^9 W/cm^2, which was much higher than the threshold fluence of the material. The distance between the focusing lens and the sample was kept less than the focal length of the lens to prevent air breakdown. The sample was mounted on a movable XYZ stage. The sample was rotated on stage to avoid deep craters on the surface of the sample. The light emitted from the plasma plume was captured by placing an optical fiber (high-OH, core diameter: 600 μm), with a collimating lens (0–45°), near the sample. The optical fiber was coupled with the LIBS

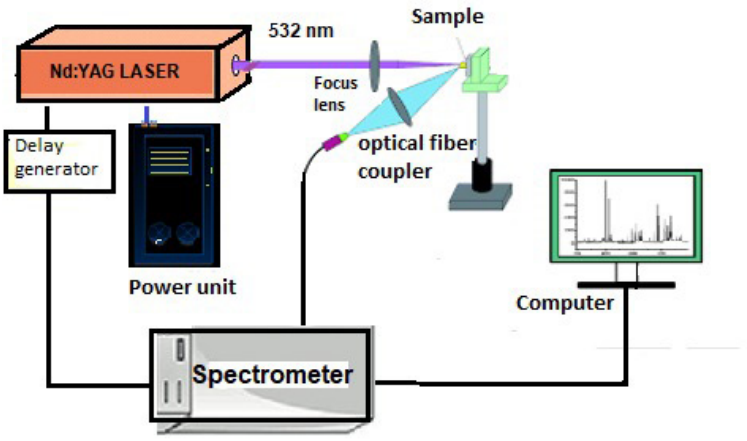

Fig. 1. Schematic diagram of the LIBS experimental set-up.

detection system, this system consisted of five spectrometers, each equipped with 2400 line/mm holographic gratings of 5-mm slit width and covering the range between 200 and 700 nm. Each spectrometer had a spectral resolution of about 0.05 nm. The integration time was about 2 ms. To record the emission spectrum, the Qswitch of the Nd:YAG laser triggers a four-channel digital delay generator (SRS DG 535), and spectrometer was triggered by the delay generator. A delay between the laser pulse and the data acquisition can be varied through the delay generator. A series of spectra were recorded at different delays between the laser pulse and the data acquisition system. The output data were averaged for three laser shots to minimize the statistical errors. The spectra were recorded at least five times to check the reproducibility of the data. The recorded signal was corrected by subtracting the dark signal of the detector through the software. A schematic diagram showing the layout of the LIBS set up is given in Fig. 1.

Results and discussion. We recorded the LIBS spectra of 22- and 18-carat gold samples in the visible and UV wavelength regions of the electromagnetic spectrum (i.e., 200 to 720 nm). By using the National Institute Standards and Technology (NIST) database, we identified the emission lines of gold (Au) and copper (Cu) with respect to their wavelengths. All emission lines come from excited and ionic atoms of Au and Cu, which are useful in determining the elemental composition of different grades of gold. Figure 2 shows the LIBS emission spectrum of 22-carat gold in UV (240 to 276 nm) and visible (464 to 505 nm) regions.

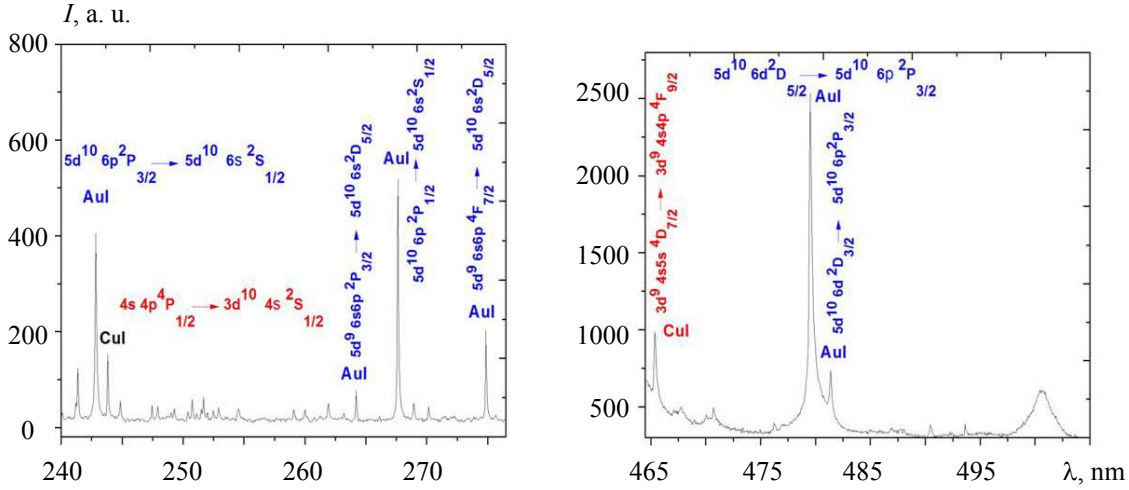

Fig. 2. Spectrum of the 22-carat gold in visible and UV wavelength regions. The peaks of Au I and Cu I are shown in blue and red, respectively.

We extended our probe into the optimization of some other key parameters. One of them was the defocusing effect of the laser light. The focusing of the laser was changed by displacing the lens forward and back of the focus on the surface of the gold alloy with the result that the power density on the targeted surface fluctuated. The optical trends for different lens-to-sample separations were almost the same. In the experiment, an intensity peak was noticed indicating that the emission signal was shot up when the laser light converged at 20 cm above the sample surface. Later, the emission spectra of gold were also observed as a function of laser power. In single-pulse mode, the effect of laser energy on the signal intensity has been observed. It is concluded that the signal intensity of peak is proportional to laser energy by keeping the distance between sample and detector fixed. To avoid under- and overestimation in plasma parameters of gold alloy samples, the intensity of spectral lines was corrected using the internal reference self-absorption correction (IRSAC) method [16, 17]. To obtain the corrected line intensities, the self-absorption absorption coefficient of observed lines used in analysis were determined and this self-absorption coefficient was divided by the observed line intensities [18]. The contribution of self-absorption in spectra appeared to be nominal because small variations in spectral lines were found. Furthermore, spectral lines involving the ground state were excluded because these lines could be severely affected by the self-absorption phenomenon [18].

Determination of plasma temperature and number density. First, we characterized the time-evolving laser-induced plasma of 22-carat gold alloy in terms of its temperature and number density. Based on the work of Griem [19] plasma temperature of species in carat gold plasma can be determined from the Boltzmann plots by using atomic parameters from the NIST database.

If plasma is in the state of local thermodynamic equilibrium (LTE), the total line intensity of the emitted line can be written as

$$\overline{I}_{ki} = Fn_z^{\alpha} A_{ki}^{\alpha} \frac{hc}{\lambda_{ki}} \frac{g_k^{\alpha}}{P_z^{\alpha}(T)} \exp\left[-\frac{E_k}{k_{\beta} T}\right], \quad (1)$$

where $\overline{I}_{ki}$ represents the integrated line intensity, n_z^{α} means the number density of species in state Z, A_{ki}^{α} means the transition probability, g_k^{α} is the k level statistical weight, K_B means the Boltzmann constant, T means the plasma temperature, $P_z^{\alpha}(T)$ means the partition function of emitting species, and F is the experimental factor that takes into account the consideration of efficiency of the detection system. By introducing a logarithm on both sides

$$\ln\left[\frac{\lambda_{ki}\overline{I_{ki}}}{hcA_{ki}g_k}\right] = -\frac{E_k}{k_{\beta}T} + \ln\left[\frac{FC_s}{U_s(T)}\right]. \quad (2)$$

Comparing Eq. (2) with a linear form of the following equation $y = mx + q_s$. Then, $y = \ln\left[\frac{\lambda_{ki}\overline{I_{ki}}}{hcA_{ki}g_k}\right]; x = E_k; m = -\frac{1}{k_{\beta}T}; q_s = \ln\left[\frac{FC_s}{U(T)}\right]$, while drawing the Boltzmann plot energy of the upper level taken along the x-axis and $\ln\left[\frac{\lambda_{ki}\overline{I_{ki}}}{hcA_{ki}g_k}\right]$ taken along the y-axis. As $m = -1/k_{\beta}T$, therefore, the plasma temperature T is derived from the slope of the Boltzmann plot. Although in the conventional CF-LIBS the concentration of all elements C_s can be predicted using the intersection value q_s of the linear regression in the Boltzmann plane:

$$C_s = \frac{U_s(T)}{F} e^{q_s}. \quad (3)$$

It is necessary to draw a Boltzmann plot of each species of the same element. The factor F can be found by normalizing the sum of all species concentrations: $\Sigma C_s = \frac{1}{F}\sum U_s(T)e^{qs} = 1$, where the s' index represents all the elements that are not negligible.

Therefore, using the conventional CF-LIBS approach, 18- and 22-carat gold alloys have compositions of Au (71.08 and 83.12%) and Cu (28.92 and 16.8%), respectively.

Plasma temperatures of Au and Cu in the 22-carat gold plasma have been estimated using Boltzmann plots, as shown in Fig. 3. To draw Boltzmann plots of neutral species, five peaks of Au I (264.29, 274.82, 312.28, 479.47, and 481.16 nm) and Cu I (324.75,406.26, 427.51, 450.94, and 465.33 nm) were used. Similarly, the wavelengths of 329.09, 331.07, 338.21, 455.80, and 506.65 nm were employed to find the plasma temperature of ionic copper. Spectroscopic parameters necessary for the determination of temperature were collected from the NIST database. Plasma temperature for neutral gold lines is about 5800±580 K whereas the plasma temperature of neutral and ionic copper lines is about 5600±560 and 5900±590 K, respectively.

Owing to the temperature heterogeneity in the laser-produced plasma, the emission of atoms and ions may form the spatial zones, which can be taken into account when using the Saha equation. For this reason, we have taken the average plasma temperature with (10% uncertainty) obtained from neutral as well as ionized spectral lines. Also, if the neutral and singly ionized transitions of each element are present in the emission spectrum and atomic parameters of these lines are also available from the literature, then we can easily determine the densities of the neutral and ionic species in two charged states, z and (z+1). In that case we can measure the plasma temperature and densities of neutral as well as the ionized species separately. But in our case, it was not possible, so we have used the Saha–Boltzmann equation, which relates to the number density of a particular element in the two consecutive charged states, z and (z+1), and which takes into account neutral as well as ionized species. This is a well-known method and has also been previously reported by many authors [20].

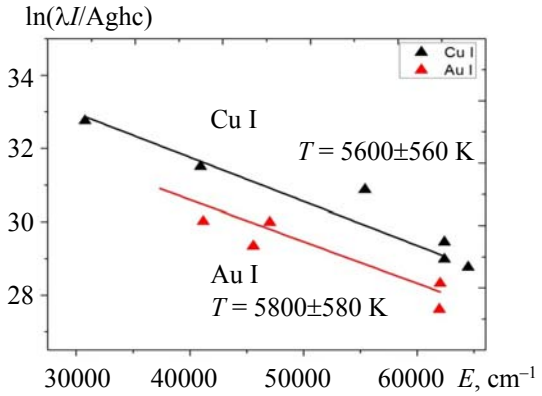

Fig. 3. Combined Boltzmann plots using lines of neutral gold (Au I) and copper (Cu I).

After the estimation of plasma temperature, the electron density, n_e, was deduced from the Saha–Boltzmann equation, which is given as [11, 19]:

$$n_e = 6.04\times10^{21}(T_{\mathrm{eV}})^{3/2}\frac{I'_z}{I'_{z+1}}\exp\left[\frac{-E_{k,\alpha,z+1}+E_{k,\alpha,z}-\chi_{\alpha,z}}{k_BT}\right], \quad (4)$$

where $E_{k,\alpha,z}$ is the upper energy level of the element α in the charged state z, $E_{k,\alpha,z+1}$ is the upper energy level of the element α in the charge state (z+1), $\chi_{\alpha,z}$ is the ionization energy of the species in the ionization state Z, and I_z is the measured intensity and it can be estimated as $I_z' = \lambda_{ki}I_{ki}/A_{ki}g_k$. The electron number densities of Au I and Cu I estimated in the 22-carat gold sample with the help of Eq. (4) were determined to be of the order of 2.71×10^{16} and 1.12×10^{16} cm^{-3}, respectively.

As laser erosion plasma (plasma of the laser plume) is very heterogeneous in both the axial and the transversal directions of the plume, obtaining local parameters of the plasma by one of the tomography techniques is a very difficult task, also taking into account very fast and strong evolution of the laser plume during its rather short lifetime from excitation to complete recombination. The elemental analysis by radiation spectra is almost justified. However, for compositional analysis uncertainties still exist, and these errors may be in the form of systematic uncertainties in transition probability, plasma temperature, and END, etc. For this reason, all the plasma parameters are calculated with 10% uncertainties.

Electron number density conservation modeling. Using the experimental data, quantitative analysis was carried out by END conservation methodology [11, 21]. It is some type of electron density comparison process. In this method, an algorithm is developed where the concentration of elements in the sample is predicted by matching the theoretically derived ratios of ENDs and the experimentally observed ratios of the number densities of identical elements as well as the different elements using the spectral line intensities. The basic requirement of this method is that the spectral lines used for the purposes of analysis should justify the LTE criterion and the plasma should be optically thin [22, 23].

We discussed the prerequisite McWhirter criterion whether the laser-induced plasma is in LTE using the formula $N_e \geq 1.6\times10^{12}T^{1/2}(\Delta E)^3$ [24]. We verified the LTE condition for Au I transitions 274.82- and 312.28-nm spectral lines having differences in energy levels ΔE = 4.52 and 3.969 eV, respectively. Although the plasma temperature recorded for Au I is taken as 5800 K, our estimated values of Au are in 10^{16} cm^{-3}, which is much higher than the value calculated from the above inequality (10^{15} cm^{-3}). Our END conservation approach is also based on another prerequisite criterion and that is the assumption of optically thin plasma, as shown in the following equation:

$$\frac{I_1}{I_2} = \frac{\lambda_2}{\lambda_1}\frac{A_1}{A_2}\frac{g_1}{g_2}\exp\left[\frac{E_2-E_1}{k_BT}\right], \quad (5)$$

where all the terms have the usual meanings. Selected spectral lines for optical thin plasma are 274.82, 312.28, and 479.21 nm for Au I, and 324.75, 406.26, and 465.33 nm for Cu I.

For compositional analysis using the LIBS plasma it is mandatory that laser-induced plasma should be optically thin. The lifetime of a plasma plume is a few milliseconds, but we do not record the entire continuum (data from the generation of plasma to the end). A time window during which our plasma was optically

thin and satisfied the condition of LTE was selected using the optimized conditions. In this way, emission spectra of only a selected portion were considered.

Besides the previous prerequisite criterion, the condition of LTE in heterogeneous plasma was also checked using a parameter called diffusion length. The diffusion of heat and mass plays a pivotal role in the evolution of laser-induced plasma. The diffusion length LD was estimated using the following relation [25, 26]:

$$LD \approx \left(1.4\times10^{12}\right)\left(\frac{(KT)^{3/2}}{n_e}\right)\left(\frac{\Delta E}{M_A f_{12}(\bar{g})}\right)^{1/2} e^{\Delta E/2KT}. \quad (6)$$

The diffusion length LD was estimated as 0.0012 cm, which is much smaller than the characteristic variation length d = 0.21 cm. Therefore, the estimation fulfilled the following criteria, i.e., 10LD < d, and it could be assumed that the plasma was very close to LTE. As the above two conditions have been satisfied, we can proceed to the END conservation modeling.

If the neutral and singly ionized transitions of each element are present in the emission spectrum and atomic parameters of these lines are also available from the literature, then we can easily determine the densities of the neutral and ionic species in two charged states z and (z+1). In that case, we can measure the plasma temperature and densities of the neutral as well as the ionized species separately. But in our case it was not possible to draw a Boltzmann plot for neutral or ionized species of an element, so we used the Saha–Boltzmann equation, which relates to the number density of a particular element in the two consecutive charged states z and (z+1). And we have utilized the average plasma temperature obtained with 10% uncertainties, which takes into account neutral as well as ionized species. This is a well-known method and has also been previously reported by many authors.

Experimental evaluation of density ratios. The density ratio of species of the same elements in two consecutive charge states using experimentally estimated values of T and n_e can be deduced using the Saha Eq. (7) as:

$$n_e \frac{n_{z+1}^{\alpha}}{n_z^{\alpha}} = 6.04\times10^{21}(T_{\mathrm{eV}})^{3/2}\frac{P_{z+1}^{\alpha}}{P_z^{\alpha}}\exp\left[-\frac{\chi_{\alpha,z}}{k_B T}\right], \quad (7)$$

where n_e (cm^{-3}) is the electron density, n_{z+1}^{α} is the density of atoms in the upper charged state (z+1) of the element α, $n_z{}^{\alpha}$ is the density of atoms in the lower charged state z of the same element α, $\chi_{\alpha,z}$ (eV) is the ionization energy of the element α in the charge state z, P_{z+1}^{α} and $P_z{}^{\alpha}$ are the partition functions respectively of the upper charged state (z + 1) and of the lower charge state z, and T_{eV} is the plasma temperature in electron volts.

The density ratio of the species of two different elements α and β can be calculated by the Saha–Boltzmann Eq. (8) as [11]:

$$\frac{n_z^{\alpha,z}}{n_{z+1}^{\beta}} = \frac{I'_{\alpha,z}}{I'_{\beta,z+1}}\frac{P_{\alpha}^{z}}{P_{\beta}^{z+1}}\exp\left[\frac{-E_{k,\beta,z+1}+E_{k,\alpha,z}}{k_B T}\right], \quad (8)$$

where all the terms have the usual meanings.

The Saha–Boltzmann equation is utilized to get more accurate contributions of neutral as well as ionized species in the plasma. In order to overcome the uncertainties in the results, we have utilized a theoretical model (END conversion method). The purpose of this method is to construct and utilize the formulas to calculate the theoretical values of n_e and the ratio of the number densities of the same elements, as well as the ratio of the number densities of different elements. The procedure is based on the following steps:

1) Initially, we suppose the values of total number density and density of species present in the sample.

2) We start an algorithm to converge these values that may be possible from our experimental conditions.

3) We calculate the total densities of neutral as well as ionized species.

4) Then we use theoretical supposed values of END, species number densities, and density ratios, and again, an algorithm starts that matches the experimental and theoretical density ratios and total number density.

5) From the density ratios, we extract the value of densities of the species present in the sample.

6) In this way, we can get more accurate values of the densities of the atomic and ionic species.

Actually, from this method we predict the more accurate values of densities of ionic and neutral species compared with the combination of the Boltzmann equation and Saha–Boltzmann equations.

Theoretical evaluation of density ratios and quantitative elemental analysis. We constructed a formula to calculate the theoretical values of n_e and the ratio of the number densities of the same elements as well as the ratio of the number densities of different elements. If n_e is the total END of the plasma and n_e^{α} is the electron density contribution from the element α to the total electron density n_e, then n_e^{α} is defined as the sum of the contribution of all ionic states of the element α as

$$n_e^{\alpha} = n_1^{\alpha} + 2n_2^{\alpha} + 3n_3^{\alpha} ... = \sum_{z=1}^{N} z n_z^{\alpha} . \tag{9}$$

If there are M elements, total electron density n_e will be defined as

$$n_e = \sum_{\alpha=1}^{M} n_e^{\alpha} . \tag{10}$$

The total number density n_{tot}^{α} is the sum of number densities of the neutral and ionized atoms of the element α, which is stated as

$$n_{\text{tot}}^{\alpha} = n_0^{\alpha} + n_1^{\alpha} + n_2^{\alpha} + ... + n_Z^{\alpha} = n_0^{\alpha}\left[1 + \sum_{z=1}^{Z_N}\left(\frac{n_z^{\alpha}}{n_0^{\alpha}}\right)\right], \tag{11}$$

where n_z^{α} means the number density of the element α in the charged state z ($z = 0$ for neutral atoms, $z = 1$ for singly ionized atoms, $z = 2$ doubly ionized atoms, and so on). Equation (9) exhibits that each singly ionized atom will contribute one electron to the total END, doubly ionized atoms contribute two electrons, and so on. Equation (11) can be written as

$$n_{\text{tot}}^{\alpha} = n_1^{\alpha}\left[1 + \frac{n_2^{\alpha}}{n_1^{\alpha}} + \frac{n_3^{\alpha}}{n_1^{\alpha}} + \cdots\right] = n_1^{\alpha}\left[1 + \sum_{z=1}^{N}\frac{n_{z+1}^{\alpha}}{n_1^{\alpha}}\right]. \tag{12}$$

Now we have to define two new functions S_z^{α} and R_z^{α}:

$$S_z^{\alpha} = n_e \frac{n^{\alpha,z+1}}{n^{\alpha,z}} = 6.04\times10^{21}(T_{\text{eV}})^{3/2}\frac{P_{z+1}^{\alpha}}{P_z^{\alpha}}\exp\left[-\frac{\chi_{\alpha,z}}{k_B T}\right]. \tag{13}$$

A new function R_z^{α} can be defined with the help of the Saha–Boltzmann equation, which relates to the ionization state and neutral state of the atom as

$$R_z^{\alpha} = \frac{n_z^{\alpha}}{n_0^{\alpha}}, R_{z+1}^{\alpha} = \frac{n_{z+1}^{\alpha}}{n_1^{\alpha}} . \tag{14}$$

The function R_z^{α} can be restated as

$$R_z^{\alpha} = \frac{n_z^{\alpha}}{n_0^{\alpha}} = \frac{n_1^{\alpha}}{n_0^{\alpha}}\times\frac{n_2^{\alpha}}{n_1^{\alpha}}\times\cdots\cdots\times\frac{n_z^{\alpha}}{n_{z-1}^{\alpha}} = \frac{S_1^{\alpha}}{n_e}\times\frac{S_2^{\alpha}}{n_e}\times\cdots\cdots\times\frac{S_z^{\alpha}}{n_e} . \tag{15}$$

The following terms n_e^{α}, n_z^{α}, $n_z^{\alpha} / n_{z+1}^{\beta}$ can be stated in terms of R_z^{α} as

$$n_e^{\alpha} = \frac{n_{\text{tot},\alpha}\sum_{z=1}^{N} Z R_z^{\alpha}}{1 + \sum_{z=1}^{N} R_z^{\alpha}} , \tag{16}$$

$$n_z^{\alpha} = \frac{n_{\text{tot}}^{\alpha}}{1 + \sum_{z=1}^{N} R_z^{\alpha}} \times R_z^{\alpha} , \tag{17}$$

$$\frac{n_z^{\alpha}}{n_{z+1}^{\beta}} = \frac{n_0^{\alpha}}{n_1^{\beta}}\frac{R_z^{\alpha}}{R_{z+1}^{\beta}} , \tag{18}$$

$$n^{\alpha,z+1} = n^{\alpha,1}\times R^{\alpha,z+1} = \frac{n_{\text{tot},\alpha}}{1 + \sum_{z=1}^{N} R^{\alpha,z+1}}\times R^{\alpha,z+1} . \tag{19}$$

If there are only two elements, Au and Cu, then the total END n_e can be calculated using Eq. (10), which can be written as

$$n_e = n_e^{\text{Au}} + n_e^{\text{Cu}} . \tag{20}$$

The END is found from Eq. (4) using intensity ratios of concerned species. The value n_e in the 22- and 18-carat plasma was determined to be 2.1×10^{16} and 1.12×10^{16} cm^{-3}, respectively. The calculated density ratios $n_{\mathrm{CuII}}/n_{\mathrm{CuI}}$ for the 22-carat and 18-carat gold plasma from Eq. (7) using the estimated value of T, n_e, and the corresponding partition function from the NIST database were found to be 52.4 and 66.1, respectively. Although the density ratio $n_{\mathrm{AuI}}/n_{\mathrm{CuII}}$ of the 22- and 18-carat gold plasma was also found from Eq. (8), which was estimated to be 0.021 and 0.013, respectively. We have also developed an algorithm explained in the flow chart diagram (Fig. 4). The values $n_{\mathrm{tot}}^{\mathrm{Au}}$ and $n_{\mathrm{tot}}^{\mathrm{Cu}}$ fluctuated within a range 10^{14}–10^{17} cm^{-3} in the algorithm and determined theoretical values n_{e}, $n_{\mathrm{CuII}}/n_{\mathrm{CuI}}$, and $n_{\mathrm{AuI}}/n_{\mathrm{CuII}}$, which should match the values of experimental density ratios at some specific values $n_{\mathrm{tot}}^{\mathrm{Au}}$ and $n_{\mathrm{tot}}^{\mathrm{Cu}}$. Later, we used the values of electron densities $n_{\mathrm{tot}}^{\mathrm{Au}} = 9.8\times10^{16}$ cm^{-3} and $n_{\mathrm{tot}}^{\mathrm{Cu}} = 1.15\times10^{16}$ cm^{-3} in a 22-carat gold sample and $n_{\mathrm{tot}}^{\mathrm{Au}} = 7.8\times10^{16}$ cm^{-3} and $n_{\mathrm{tot}}^{\mathrm{Cu}} = 3.41\times10^{16}$ cm^{-3} in a 18-carat gold sample for estimation of elemental composition. Substituting these values in the Eqs. (21) and (22), the weight concentrations were calculated to be Au (88.32%) and Cu (10.68%) for the 22-carat gold. Similarly, we determined the weight concentrations of Au and Cu in the 18-carat gold. Therefore, using the END conservation approach for LIBS, the 18-carat gold composition of Au was 73.48% and for Cu it was 26.52%. The calculated concentration of Au and Cu in the 22-carat and 18-carat gold samples obtained from the END conservation LIBS, along with their certified values, are shown in Table 1. This END conservation modeling turned out to be a successful analytical solution for gold alloys.

$$C^{\mathrm{Au}} = \frac{n_{\mathrm{tot}}^{\mathrm{Au}}}{n_{\mathrm{tot}}^{\mathrm{Au}} + n_{\mathrm{tot}}^{\mathrm{Cu}}} \times 100\% , \tag{21}$$

$$C^{\mathrm{Cu}} = \frac{n_{\mathrm{tot}}^{\mathrm{Cu}}}{n_{\mathrm{tot}}^{\mathrm{Au}} + n_{\mathrm{tot}}^{\mathrm{Cu}}} \times 100\% . \tag{22}$$

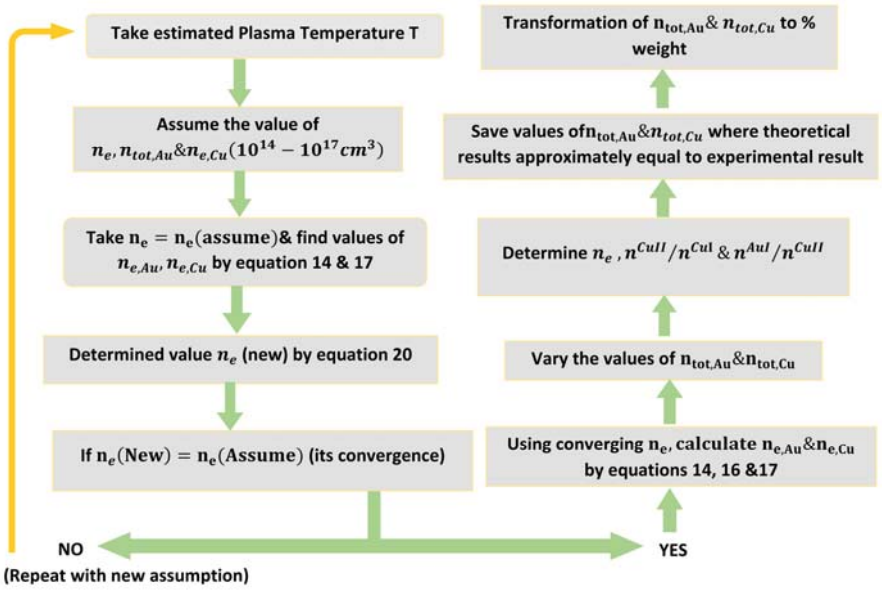

Fig. 4. Flow chart of essential steps involved in the implementation of a model in the theoretical calculations of density ratios.

TABLE 1. The Comparison of the END Conservation-LIBS and CF-LIBS Methods with Standard Recognized Techniques Used for the Quantitative Analysis of Carat Gold

Certified concentration, wt%		Concentration (wt%) by conventional CF-LIBS, %		Concentration (wt%) by END conservation-LIBS, %		Concentration (wt%) by EDX, %	
Au	Cu	Au	Cu	Au	Cu	Au	Cu
91.6	8.4	83.12	16.88	88.32	11.68	90.62	9.38
75	25	71.08	28.92	73.48	26.52	74.11	25.89

Comparison of the END conservation LIBS technique with EDX. Two samples of gold (i.e., 22- and 18-carat) were investigated by the END conservation LIBS and compared with the conventional CF-LIBS approach. Using the conventional CF-LIBS, the contents of Au and Cu in 22-carat gold alloy were estimated to be 83.12 and 16.88%, respectively. In the conventional CF-LIBS, some uncertainty has been monitored for gold alloys because some dependencies existed. The results of the conventional CF-LIBS are dependent upon slopes and intercepts of Boltzmann plots and a small deviation in these parameters adversely affects the quantitative results. Sometimes it is hard to make the Boltzmann plots for all the constituents present in the sample because of fewer lines in the emission spectra. Therefore, the results for conventional CF-LIBS may be uncertain. Compared with the conventional CF-LIBS, the END conservation approach was more efficient.

The results of the END conservation LIBS were also compared with other established multivariate methodologies, such as energy dispersive X-ray (i.e., EDX). EDX is an analytical methodology employed for compositional analysis. The technique resolves the 22-carat gold sample with the composition of Cu (9.38%) and Au (90.62%), whereas it resolves the 18-carat gold sample with a composition of Au (74.11%) and Cu (25.89%), respectively, as shown in Fig. 5.

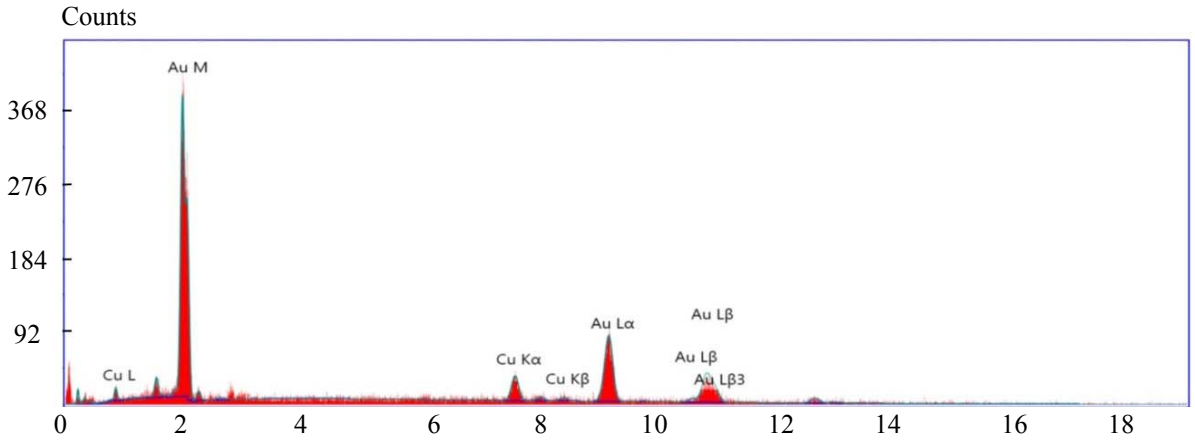

Fig. 5. The energy dispersive X-ray (EDX) spectrum of the 22-carat gold.

For validated compositions of gold, a handsome correlation between the END conservation LIBS methodology and standard recognized techniques has been observed. Table 1 shows that the results obtained from the END conservation LIBS are comparable with results obtained by EDX.

Conclusions. Laser-induced plasma was characterized in terms of its temperature and electron number density using LIBS. The LIBS experiment was designed to investigate the content of gold and copper in 22- and 18-carat gold alloys. We combined the basic LIBS procedure with the electron number density conservation approach for the compositional analysis of gold alloys. The electron number density conservation methodology was applied on the LIBS spectrum, which is based on the theory of electron number density. The density ratios of Au and Cu using the line intensities of the species in different charge states of Au and Cu were determined experimentally as well as theoretically. An algorithm has been developed for the quantitative analysis of gold alloys and the compositions of Au and Cu in the carat gold samples were determined. To compare analytical ability of the electron number density conservation LIBS approach with other frequently used calibration free techniques, quantitative analysis was also carried out using the conventional CF-LIBS. The composition analysis of gold alloys obtained from the electron number density observation LIBS agreed well with the conventional CF-LIBS and certified values of gold alloys. Results ensured that the END conservation modeling is significantly better than the conventional CF-LIBS methodology and is comparable with the established analytical technique, EDX.

Acknowledgments. Financial support for this work was provided by the Higher Education Commission of Pakistan (NRPU Project No. 8884).

REFERENCES

1. L. J. Radziemski, D. A. Cremers, *Handbook of Laser-Induced Breakdown Spectroscopy*, John Wiley & Sons, **1**, 1–4 (2006).
2. M. Fahad, Z. Farooq, M. Abrar, *Appl. Opt.*, **58**, No. 13, 3501–3508 (2019).
3. C. Aragon, J. A. Aguilera, F. Penalba, *Appl. Spectrosc*., **53**, No. 10, 1259–1267 (1999).
4. P. Fichet, D. Menut, R. Brennetot, E. Vors, A. Rivoallan, *Appl. Opt.*, **42**, No. 30, 6029–6035 (2003).
5. V. Burakov, S. Raikov, *Spectrochim. Acta B: At. Spectrosc.*, **62**, No. 3, 217–223 (2007).
6. E. Tognoni, G. Cristoforetti, S. Legnaioli, V. Palleschi, A. Salvetti, M. Müller, U. Panne, I. Gornushkin, *Spectrochim. Acta B: At. Spectrosc*., **62**, No. 12, 1287–1302 (2007).
7. A. Ciucci, M. Corsi, V. Palleschi, S. Rastelli, A. Salvetti, E. Tognoni, *Appl. Spectrosc*., **53**, No. 8, 960–964 (1999).
8. J. Yang, X. Li, J. Xu, X. Ma, *Appl. Spectrosc*., **72**, No. 1, 129–140 (2018).
9. Z. Farooq, R. Ali, U. S. Qurashi, M. H. Mahmood, M. Yaseen, M. A. Qayyum, M. N. Hussain, S. M. Shah, T. Jan, *Phys. Plasmas*, **25**, No. 9, 093106 (2018).
10. M. Fahad, Z. Farooq, M. Abrar, K. H. Shah, T. Iqbal, S. Saeed, *Laser Phys*., **28**, No. 12, 125701 (2018).
11. J. Gomba, C. D'Angelo, D. Bertuccelli, G. Bertuccelli, *Spectrochim. Acta B: At. Spectrosc*., **56**, No. 6, 695–705 (2001).
12. V. V. Kogan, M. W. Hinds, G. I. Ramendik, *Spectrochim. Acta B: At. Spectrosc*., **49**, No. 4, 333–343 (1994).
13. S. H. Langer, A. Saud, G. McDonald, J. A. Koutsky, Google Patents (1987).
14. M. Heurtebise, F. Montoloy, J. Lubkowitz, *Anal. Chem*., **45**, No. 1, 47–52 (1973).
15. W. Stankiewicz, B. Bolibrzuch, M. Marczak, *Gold Bull*., **31**, No. 4, 119–125 (1998).
16. L. Sun, H. Yu, *Talanta*, **79**, No. 2, 388–395 (2009).
17. A. El Sherbini, T. M. El Sherbini, H. Hegazy, G. Cristoforetti, S. Legnaioli, V. Palleschi, L. Pardini, A. Salvetti, E. Tognoni, *Spectrochim. Acta B: At. Spectrosc*., **60**, No. 12, 1573–1579 (2005).
18. Z. Farooq, R. Ali, A. Ali, T. Mubeen, T. Jan, H. Anwar, *Appl. Spectrosc*., **73**, No. 1, 30–39 (2019).
19. H. Griem, Monographs on Plasma Physics, Cambridge, Cambridge University Press, **55**, 59–61 (1997).
20. Q. Abbass, N. Ahmed, R. Ahmed, M. A. Baig, *Plasma Chem. and Plasma Proc*., **36**, No. 5, 1287–1299 (2016).
21. V. Unnikrishnan, K. Mridul, R. Nayak, K. Alti, V. Kartha, C. Santhosh, G. Gupta, B. Suri, *Pramana*, **79**, No. 2, 299–310 (2012).
22. V. Unnikrishnan, K. Alti, V. Kartha, C. Santhosh, G. Gupta, B. Suri, *Pramana*, **74**, No. 6, 983–993 (2010).
23. Z. Farooq, R. Ali, A. ul Ahmad, M. Yaseen, M. H. Mahmood, M. Fahad, M. N. Hussain, I. Rehan, M. Z. Khan, M. U. Farooq, *Appl. Opt*., **59**, No. 8, 2559–2568 (2020).
24. R. McWhirter, presented at the Plasma diagnostic techniques, 1965 (unpublished).
25. G. Cristoforetti, A. De Giacomo, M. Dell'Aglio, S. Legnaioli, E. Tognoni, V. Palleschi, N. Omenetto, *Spectrochim. Acta B: At. Spectrosc*., **65**, No. 1, 86–95 (2010).
26. G. Cristoforetti, E. Tognoni, L. A. Gizzi, *Spectrochim. Acta B: At. Spectrosc*., **90**, 1–22 (2013).